

ORIGIN OF RADIALLY ALIGNED MAGNETIC FIELDS IN YOUNG SUPERNOVA REMNANTS

TSUYOSHI INOUE¹, JIRO SHIMODA¹, YUTAKA OHIRA¹, AND RYO YAMAZAKI¹

Draft version September 30, 2022

ABSTRACT

It has been suggested by radio observations of polarized synchrotron emissions that downstream magnetic field in some young supernova remnants are oriented radially. We study magnetic field distribution of turbulent supernova remnant driven by the Richtmyer-Meshkov instability – in other words, the effect of rippled shock – by using three-dimensional magnetohydrodynamics simulations. We find that the induced turbulence has radially biased anisotropic velocity dispersion that leads to a selective amplification of the radial component of the magnetic field. The Richtmyer-Meshkov instability is induced by the interaction between the shock and upstream density fluctuations. Future high-resolution polarization observation can distinguish the following candidates responsible for the upstream density fluctuations: (i) inhomogeneity caused by the cascade of large-scale turbulence in the ISM so-called the big-power-law-in-the-sky, (ii) structures generated by the Drury instability in the cosmic-ray modified shock, and (iii) fluctuations induced by the non-linear feedback of the cosmic-ray streaming instability.

Subject headings: ISM: supernova remnants — instabilities — magnetic fields — shock waves

1. INTRODUCTION

Supernova remnants (SNRs) are believed to be the sites of galactic cosmic-ray acceleration by the diffusive shock acceleration (DSA; Bell 1978; Blandford & Ostriker 1978). However, owing to large ambiguity of magnetic field which plays essential role in the DSA by scattering particles, detailed process of the DSA remains a matter of debate. Polarization observations of synchrotron emissions can be crucially important, since they have variety of information about the magnetic field in the SNRs. It has been suggested by radio polarization observations that the magnetic fields in some young SNRs are oriented radially (Dickel et al. 1991 for Tycho’s SNR; DeLaney et al. 2002 for Kepler’s SNR; Dickel & Milne 1976, Reynolds & Gilmore 1993, Reynoso et al. 2013 for SN1006).

Jun & Norman (1996) studied the Rayleigh-Taylor instability (RTI) at the contact surface in the SNR. They found that the growth of the RTI causes the radially oriented magnetic field, because the RTI driven turbulence is biased toward the radial component. Although the RTI provides a promising origin of magnetic field orientation in the SNRs, it can work only in the vicinity of the contact surface (see, however, Schure et al. 2009), while the observations suggest radial orientation even in the region of shocked interstellar medium (ISM) ahead of the contact (e.g., Reynoso et al. 2013). The Richtmyer-Meshkov instability (RMI; Richtmyer 1960) may solve the puzzle of the magnetic field orientation in the SNRs, because the RMI is a Rayleigh-Taylor type instability that is induced by the interaction between the shock and density fluctuations in the ISM, i.e., the RMI can grow even at the downstream of the forward shock.

The role of the RMI in the SNR has recently been studied using magnetohydrodynamics (MHD) simulations. Giacalone & Jokipii (2007) and Guo et al. (2012) studied shock propagation of an inhomogeneous ISM with the Kolmogorov-like density power spectrum, and reported that the RMI driven turbulence (in other words, the turbulence driven by the effect of rippled shock) induces small-scale dynamo effect that amplifies the magnetic field. Inoue et al. (2009; 2010; 2012) and

TABLE 1
MODEL PARAMETERS

Model No.	1	2	3	4	5	6
$\Delta\rho/\langle\rho\rangle_0$	0.3	0.3	0.1	0.5	0.7	0.8
$B_{x,0}$ [μ G]	0.0	3.0	0.0	0.0	0.0	0.0
$B_{y,0}$ [μ G]	3.0	0.0	3.0	3.0	3.0	3.0
$\langle \chi_z \rangle_{P<0.3^a}$	44°	24°	72°	37°	39°	38°
$\langle \chi_y \rangle_{P<0.3^b}$	28°	23°	36°	26°	27°	27°
$\langle P \rangle^c$	0.26	0.30	0.46	0.22	0.22	0.22
l_{tr}^d [pc]	0.33	N/A	N/A	0.26	0.23	0.23

^aaverage polarization angle to the x -axis where $P < 0.3$ observed along the z -axis.

^bsame as ^a but observed along the y -axis.

^caverage polarization degree.

^daverage distance from the shock front at which polarization angle becomes $|\chi| \leq 5^\circ$.

Sano et al. (2012) studied the magnetic field amplification by the RMI driven turbulence due to shock-cloud interaction and discussed its influence on the particle acceleration and high-energy emissions. However, the influence of the amplified magnetic field by the RMI on the polarization of synchrotron emission has not been studied so far. In this paper, by using three-dimensional MHD simulations, we study the polarized synchrotron emissions from turbulent SNR driven by the RMI.

2. SETUP OF SIMULATIONS

We solve the ideal MHD equations for the gas with adiabatic index $\gamma = 5/3$ and mean molar weight 1.27. The basic MHD equations are solved using the second-order Godunov-type finite-volume scheme (van Leer 1979) that employs an approximate MHD Riemann solver developed by Sano et al. (1999). The consistent method of characteristics with the constrained transport technique (Clarke 1996) is used for solving the induction equations that ensures the divergence free constraint. The integration is done in the conservative fashion, so that we can handle high-Mach-number shock waves precisely.

Since we consider the ideal MHD, the results of the simulations are scale-free. The physical scale is introduced when we fix the scale of density fluctuations given below. In the following, for intuitive presentation, we express the scale of the

¹ Department of Physics and Mathematics, Aoyama-Gakuin University, Sagamihara, Kanagawa 252-5258, Japan; inouety@phys.aoyama.ac.jp

system using physical scales. We prepare a cubic numerical domain of the volume $L_{\text{box}}^3 = (2 \text{ pc})^3$ that is composed of 1024^3 uniform unit cells. Because the SNRs that show radially oriented magnetic field seem to be located in the diffuse ISM, we consider so-called the "big-power-law-in-the-sky" (Armstrong et al. 1995) as an origin of the density fluctuations in the preshock ISM. The fluctuations are given as a superposition of sinusoidal functions with various wave numbers that ranges $2\pi/L_{\text{box}} \leq |k| \leq 256\pi/L_{\text{box}}$ and random phases. The power spectrum of the density fluctuations is given as the isotropic power law: $P_{\text{ID}}(k) \equiv \rho_k^2 k^2 \propto k^{-5/3}$ for the above range of k , where ρ_k is the Fourier component of the density, which is consistent with the big-power-law-in-the-sky. Thus, our initial density structure is parameterized by mean density $\langle \rho \rangle_0$ and dispersion $\Delta \rho \equiv (\langle \rho^2 \rangle - \langle \rho \rangle_0^2)^{1/2}$.

We set the mean number density to be $\langle n \rangle_0 = 0.5 \text{ cm}^{-3}$ and the initial thermal pressure to be $p/k_B = 4 \times 10^3 \text{ K cm}^{-3}$ that are typical values in the diffuse ISM (Myers 1978), and we assume the initial magnetic field strength of $B_0 = 3.0 \mu\text{G}$, which is also typical in the diffuse ISM (Beck 2000). Thus, the initial mean sound speed and Alfvén velocity are $\langle c_s \rangle_0 = 9.3 \text{ km s}^{-1}$ and $\langle c_A \rangle_0 = 8.2 \text{ km s}^{-1}$, respectively. The model parameters (the initial degree of the fluctuation and the initial orientation of magnetic field) are summarized in Table 1.

If we suppose the turbulence in the diffuse ISM is driven by supernovae, the driving-scale of the turbulence and the degree of density fluctuation at the driving-scale would be given as $L_{\text{inj}} \sim 100 \text{ pc}$ and $\Delta \rho|_{L_{\text{inj}}}/\langle \rho \rangle \sim 1$, respectively (e.g., de Avezil & Breitschwerdt 2007). In that case, the degree of small-scale density fluctuations due to cascade of the turbulence at the scale $L_{\text{box}} = 2 \text{ pc}$ is estimated as $\Delta \rho|_{L_{\text{box}}}/\langle \rho \rangle \simeq (L_{\text{box}}/L_{\text{inj}})^{1/3} \simeq 0.27$, where we have used the relation $\Delta \rho^2|_l = \int_{l/l}^{\infty} \rho_k^2 dk^3 = l^{2/3}$. Hence, we regard Models 1 and 2 as standard ISM models.

To induce a blast wave that generates a shocked layer, we set a hot plasma of $p_h/k_B = 2 \times 10^8 \text{ K cm}^{-3}$, $n_h = 0.05 \text{ cm}^{-3}$ and $B_h = 3.0 \mu\text{G}$ at the $x = 0$ boundary plane. According to the solution of the Riemann problem, when the preshock density takes uniform value of $n = 0.5 \text{ cm}^{-3}$, such a hot gas induces a shock wave of $v_{\text{sh}} = 1795 \text{ km s}^{-1}$, indicating that mean shock velocity induced by the hot gas is $\langle v_{\text{sh}} \rangle \simeq 1800 \text{ km s}^{-1}$. We use the periodic boundary conditions for the x - y and the x - z boundary planes, and we assume free boundary condition at the $x = L_{\text{box}}$ boundary plane.

3. RESULTS OF SIMULATIONS AND SYNTHETIC OBSERVATIONS

In Figure 1, we show a two-dimensional slice of the magnetic field strength (*upper half*) and the number density (*lower half*) of the result of Model 1 at $t = 700 \text{ yr}$. Interaction between the blast wave shock and the density fluctuations results in a formation of turbulent shocked slab where magnetic field is amplified beyond the shock compression value. Top panel of Figure 2 shows evolution of the average magnetic field strength $\langle |\mathbf{B}| \rangle_{\text{sl}}$ and the dispersion $\langle \mathbf{B}^2 \rangle_{\text{sl}}^{1/2}$ in the shocked layer. Here $\langle \cdots \rangle_{\text{sl}}$ represents the mean value in the shocked region where $p/k_B > 10^5 \text{ K cm}^{-3}$ and $n > 0.3 \text{ cm}^{-3}$ (the former and latter conditions exclude the preshock ISM and the hot ejecta component, respectively). One can find more detailed descriptions about the generation of turbulence by the RMI (or the effect of rippled shock in another expression) and resulting dynamo effect in many literatures (e.g., Giacalone & Jokipii 2007; Inoue et al. 2012; Frascchetti 2013).

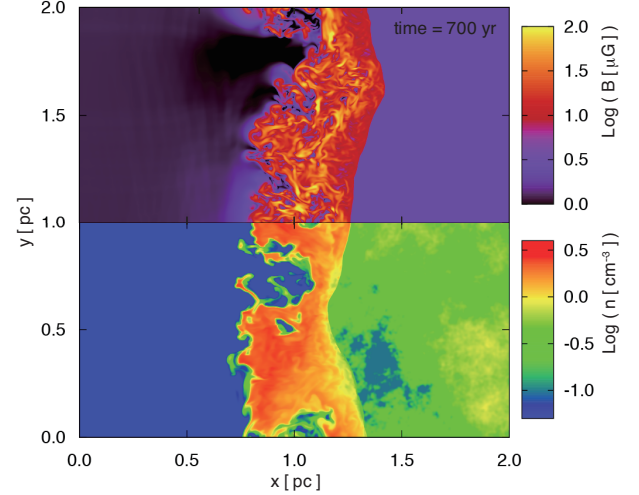


FIG. 1.— Two-dimensional slice of the magnetic field strength (*upper half*) and the number density (*lower half*) of the result of Model 1 at $t = 700 \text{ yr}$ and $z = 0 \text{ pc}$ plane.

The middle panel of Figure 2 shows, for the perpendicular shock models, the velocity dispersion in the shocked layer $\Delta v \equiv (\sum_i \langle v_i^2 \rangle_{\text{sl}} - \langle v_i \rangle_{\text{sl}}^2)^{1/2}$ and the dispersion of magnetic field strength ΔB at $t = 700 \text{ yr}$ as functions of the preshock density dispersion. If we apply the result of a simple linear analysis by Richtmyer (1960), the velocity dispersion of shocked density fluctuations that is essentially given by the growth velocity of the RMI can be written as

$$\Delta v \simeq v_{\text{RMI}} \simeq A \langle v_{\text{sh}} \rangle \eta, \quad (1)$$

where $A \simeq (\Delta \rho / \rho) / (1 + \Delta \rho / \rho)$ corresponds to the Atwood number and η corresponds to the ellipticity of the fluctuation that is unity for the isotropic inhomogeneity (see Nishihara et al. 2004; Mikaelian 1996; Inoue 2012 for more sophisticated analyses). Eq. (1) with $\langle v_{\text{sh}} \rangle = 1800 \text{ km s}^{-1}$ and $\eta = 1$ is plotted in the middle panel of Figure 2 as a solid line. We can see the good agreement between the theoretical estimation and simulations, and it is clear that Δv saturates for large $\Delta \rho / \rho$.

To calculate the polarization degree and angle of synchrotron emission from the shocked layer, we use the formulae following Clarke et al. (1989):

$$i(s) = K(\nu) \nu^{-\alpha} \{ |\mathbf{B}(s)| \sin \psi(s) \}^{1+\alpha}, \quad (2)$$

$$I = \int_{\text{l.o.s.}} i(s) ds, \quad (3)$$

$$Q = \int_{\text{l.o.s.}} f_0 i(s) \cos[2\phi(s)] ds, \quad (4)$$

$$U = \int_{\text{l.o.s.}} f_0 i(s) \sin[2\phi(s)] ds, \quad (5)$$

where $K(\nu)$ is a function depending on the density of relativistic electrons, $\alpha = (p-1)/2$ ($p = 2$ is the spectral index of the relativistic electrons by the DSA), $f_0 = (\alpha+1)/(\alpha+5/3)$ is a local linear polarization degree for isotropic electrons, ψ is an angle between local magnetic field and the line of sight, and ϕ is a position angle of the local magnetic field projected onto the plane of the sky and the x -axis. In the following, we assume that the relativistic electrons are uniformly distributed in the shocked region ($K = \text{const.}$), and we set $\alpha = 0.5$.

Figure 3 shows the structure of polarization degree $P \equiv \sqrt{Q^2 + U^2} / I$ (colors) and the magnetic field orientation vectors derived from the polarization angle $\chi = \tan^{-1}(U/Q)/2$

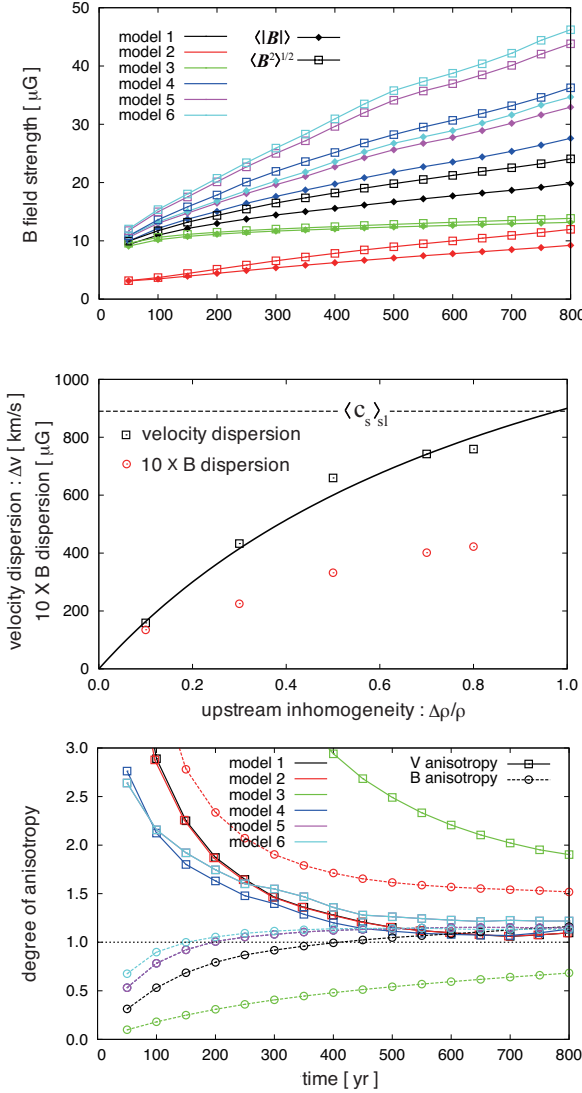


FIG. 2.— Top: Temporal evolution of the average magnetic field strength $\langle B \rangle_{sl}$ and the dispersion $\langle B^2 \rangle_{sl}^{1/2}$ in the shocked layer. Mid: Velocity dispersion Δv and the dispersion of magnetic field strength ΔB at $t = 700$ yr for the perpendicular shock cases as functions of the upstream density inhomogeneity $\Delta\rho/\rho_0$. Solid line shows a theoretical estimation of the velocity dispersion given by eq. (1), and dashed line indicates mean post-shock sound speed $\langle c_s \rangle_{sl}$. Bottom: Ratio of v_x dispersion to the average value of v_y and v_z dispersions $[r_v \equiv 2\Delta v_x/(\Delta v_y + \Delta v_z)]$ (solid) and ratio of the average strength of B_x to the average value of B_y and B_z strengths $[r_B \equiv 2\langle |B_x| \rangle_{sl}/(\langle |B_y| \rangle_{sl} + \langle |B_z| \rangle_{sl})]$ (dotted).

(bars) observed along the z -axis. Panels (a)-(d) correspond to the results of Models 1-4, respectively. We see that the orientation angle to the x -axis χ decrease with distance from the shock, even in the cases of the perpendicular shock. In particular, substantial fraction of the orientation vectors are aligned almost radially (x -direction) in the results of $\Delta\rho/\rho \geq 0.3$ (panels [a] and [d]). Note that our choice of the l.o.s. direction along z -axis corresponds to the situation in which the expectation value of the polarization angle to the x -axis $\langle |\chi| \rangle$ is the largest in any other l.o.s. direction. In Table 1, we list the average polarization angles for the cases of the l.o.s. along z -axis ($\langle |\chi_z| \rangle_{P<0.3}$) and the l.o.s. along y -axis ($\langle |\chi_y| \rangle_{P<0.3}$), in which the average is taken in the region of $P < 0.3$ where the effect of turbulence is active. In the models of $\Delta\rho/\rho \geq 0.3$, both angles are smaller than that of the isotropic case: 45° .

The mechanism for this transition of the orientation vector

can be explained as follows: In the bottom panel of Figure 2, we plot the ratio of v_x dispersion to the average value of v_y and v_z dispersions $[r_v \equiv 2\Delta v_x/(\Delta v_y + \Delta v_z)]$ (solid) and the ratio of the average strength of B_x to the average value of B_y and B_z strengths $[r_B \equiv 2\langle |B_x| \rangle_{sl}/(\langle |B_y| \rangle_{sl} + \langle |B_z| \rangle_{sl})]$ (dotted). We see that the velocity dispersion is anisotropic that is biased toward x -component. This indicates that the turbulence, which stretches and amplifies magnetic field lines, works selectively for the x -component magnetic field. As a result, the magnetic field orientation derived from the polarization angle shifts to the x -direction. This mechanism is essentially the same as the RTI case at the contact surface studied by Jun & Norman (1996), and possibly explains small dispersion of dust emission/absorption polarization angles in molecular clouds as discussed in Inoue & Inutsuka (2012). As for Model 3 ($\Delta\rho/\rho = 0.1$), the anisotropy of magnetic field strength r_B do not exceed unity in 800 yr evolution, because of the smaller velocity dispersion due to the lower upstream inhomogeneity. This results in the insufficient polarization transition in the panel (c).

In Table 1, we exhibit the mean polarization degrees $\langle P \rangle$ at $t = 700$ yr. The polarization degree of $\langle P \rangle \simeq 20\text{-}30\%$ in the shocked layer for the cases of $\Delta\rho/\rho \geq 0.3$ agrees with the radio polarization observations of young SNRs (Dickel et al. 1991; DeLaney et al. 2002; Reynolds & Gilmore 1993; Reynoso et al. 2013). These lower polarization degrees $\langle P \rangle$ compared to the homogeneous magnetic field case of $P \simeq 70\%$ for the standard DSA electron spectrum is clearly attributed to the turbulent structure of the magnetic field.

Because the transition of polarization angle is caused by the anisotropic turbulent dynamo effect, larger velocity dispersion of turbulence results in a smaller transition length of the polarization angle. The transition lengths of the polarization angle for the perpendicular shock cases are $l_{tr} = 0.33$ pc for Model 1 ($\Delta\rho/\rho = 0.3$), 0.25 pc for Model 4 ($\Delta\rho/\rho = 0.5$), 0.23 pc for Model 5 ($\Delta\rho/\rho = 0.7$), and 0.23 pc for Model 6 ($\Delta\rho/\rho = 0.8$). Here the transition length is defined as the average distance from the shock front at which polarization angle becomes $|\chi_{cr}| \leq 5^\circ$. Note that the transition lengths are converged at $t \simeq 500$ yr within $\simeq 20\%$ deviations from the above values. We also confirmed that the transition length are converged within $\simeq 20\%$ deviations, even if we employed $|\chi_{cr}| \leq 10^\circ$.

4. DISCUSSION

Can the RMI driven turbulence account for the observed radially oriented magnetic fields in the young SNRs? Recent radio polarization observation of SN1006 has shown that the magnetic field orientation in the southwest region is shifted from perpendicular (to the shock normal) to parallel (see, Figure 8 of Reynoso et al. 2013). The transition length of the polarization angle is apparently $\leq 10''$ that corresponds to $l_{tr} \leq 0.1$ pc for the distance $d = 2.18$ kpc (see, Figure 3 of Reynoso et al. 2013).

As we have discussed in §2 that the upstream density dispersion of $\Delta\rho/\rho \simeq 0.3$ (for $L_{box} = 2$ pc) may be the standard fluctuation amplitude in the diffuse ISM. If so, the transition length of the polarization angle is $l_{tr} \simeq 0.3$ pc (Table 1) that can be comparable to or slightly larger than the case of SN1006. Note that, even if the amplitude of the fluctuations is much larger ($\Delta\rho/\rho > 0.3$), the velocity dispersion of induced turbulence can be at most as large as the cases of Models 4-6, because the induced velocity dispersion saturates at $\Delta\rho/\rho \simeq 0.6$ (see, mid panel of Figure 2), which does not

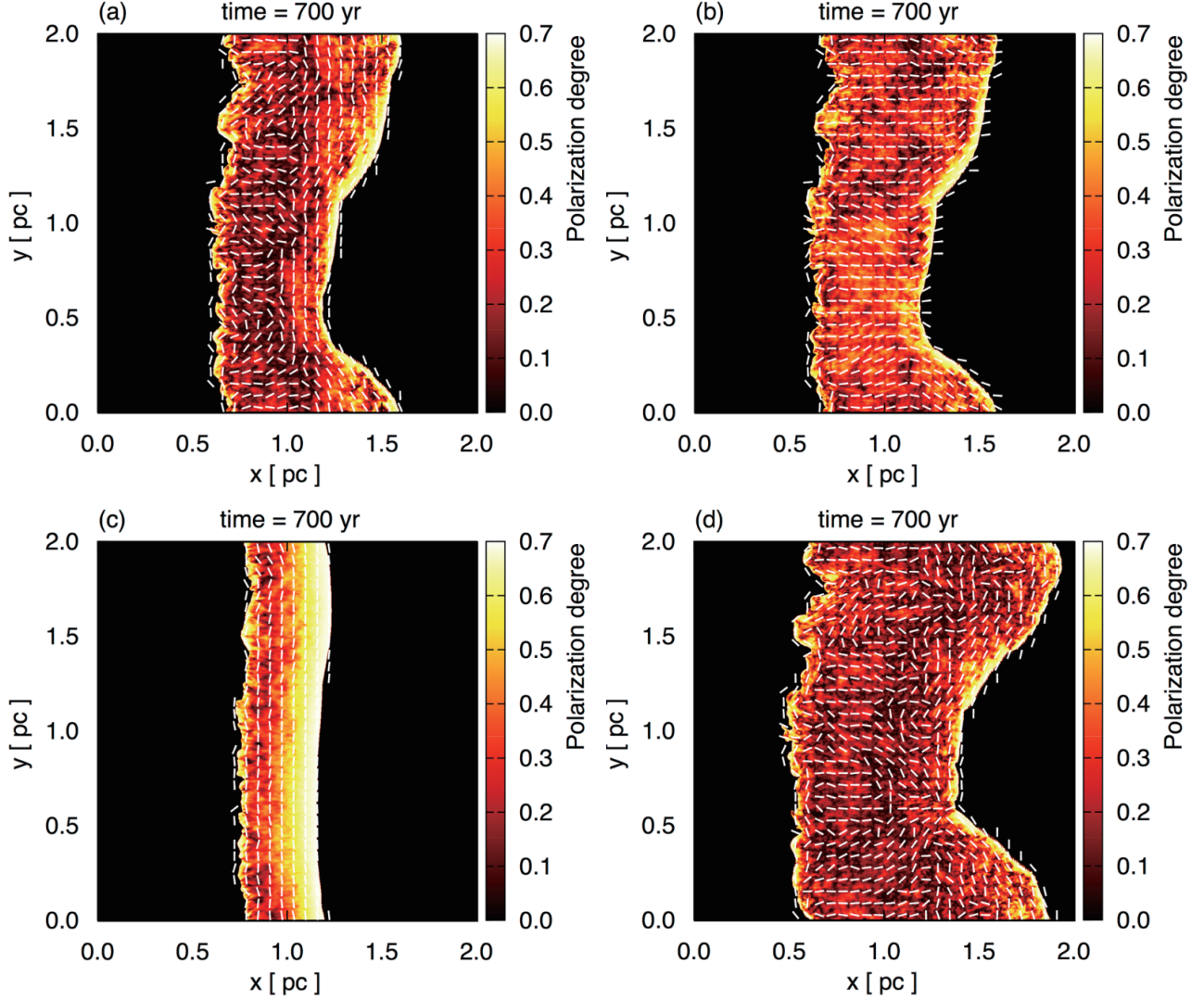


FIG. 3.— Structures of polarization degree $\sqrt{Q^2 + U^2}/I$. White bars indicate the magnetic field orientation vectors derived from the polarization angle $\chi = \tan^{-1}(U/Q)/2$. Panel (a)-(d) correspond to the results of Models 1-4, respectively. The choice of the l.o.s. along z-axis corresponds to the case in which expectation value of the polarization angle $\langle |\chi| \rangle$ takes maximum.

substantially shorten the transition length (see, Table 1).

The observed transition length of the southwest region of SN1006 can be much smaller than 0.1 pc ($10''$), since it is comparable to the scale of beam spread. In that case, we have interesting options to address the scale discrepancy between the theory and observation as follows: As we have mentioned in §2, since our mechanism is based on the scale-free ideal MHD phenomenon, we can expect smaller scale polarization shift, if there are small-scale fluctuations with sufficient amplitude. In other words, if we re-normalize the scale of our numerical domain to be 1/10th of our choice, the same result with the 1/10th of spatial and temporal scales without changing other variables is obtained. We can reasonably expect large-amplitude small-scale density fluctuations around the young SNR shock, if the cosmic-ray acceleration is efficient. For instance, if the acceleration efficiency of cosmic-rays is high enough to modify the shock wave, the Drury instability can be an origin of the large-amplitude small-scale density fluctuations, which amplifies preexistent sound waves in the precursor of the cosmic-ray modified shock (Drury & Falle 1986). Also, recent particle-in-cell simulations have shown that the cosmic-ray streaming instability (e.g., Bell

2004) causes density fluctuations in the upstream region in its non-linear stage (Riquelme & Spitkovsky 2009; Niemiec et al. 2008; Ohira et al. 2009) that can be an origin of the large-amplitude small-scale density fluctuations. In addition, the density fluctuations could be produced by pickup ions originated in hydrogen atoms (Ohira et al. 2012; Ohira 2012).

In the case of the Drury instability, the most unstable scales of the acoustic waves are (Malkov et al. 2010)

$$l_D \lesssim 4\pi\rho_{\text{up}}c_{s,\text{up}}^2/(\partial_x p_{\text{CR}}), \quad (6)$$

where $\partial_x p_{\text{CR}}$ is the cosmic-rays pressure gradient in the shock precursor. As for the non-linear stage of the cosmic-ray streaming instability, the typical scale is given by (Bell 2004)

$$l_{\text{cs}} \simeq B_{\text{up}}c/(2j_{\text{CR}}), \quad (7)$$

where $j_{\text{CR}} = en_{\text{CR}}v_{\text{sh}}$ is the cosmic-ray current density and B_{up} is the upstream magnetic field strength amplified by the instability that can be measured via the thickness of thin synchrotron shell. Because the typical scale of the RMI that roughly gives the transition length can be written as (Richtmyer 1960)

$$l_{\text{tr}} \sim v_d t_{\text{RMI}} \simeq v_d l_{\Delta\rho}/(Av_{\text{sh}}), \quad (8)$$

where v_d is the downstream velocity, $l_{\Delta\rho}$ is the typical scale of the density fluctuation, and $A \simeq (\Delta\rho/\rho)/(1 + \Delta\rho/\rho)$ is the Atwood number. Thus, once the scale of the transition length is measured with sufficient resolution, we can recover the scale of the Drury instability or the cosmic-ray streaming instability by substituting l_D or l_{cs} for $l_{\Delta\rho}$ that potentially enable us to measure the cosmic-ray pressure gradient: $\partial_x p_{CR} \sim 4\pi v_d \rho_{up} c_{s,up}^2 / (A v_{sh} l_{tr})$ or the cosmic-ray number density: $n_{CR} \sim v_d B_{up} c / (2A e v_{sh}^2 l_{tr})$, respectively.

Numerical computations were carried out on XC30 system at the Center for Computational Astrophysics (CfCA) of National Astronomical Observatory of Japan and K computer at the RIKEN Advanced Institute for Computational Science (No. hp120087). This work is supported by Grant-in-aids from the Ministry of Education, Culture, Sports, Science, and Technology (MEXT) of Japan, No. 23740154. T. I. and R. Y. deeply appreciate Research Institute, Aoyama-Gakuin University for helping and progressing our research by the fund.

REFERENCES

- Armstrong, J. W., Rickett, B. J., & Spangler, S. R. 1995, *ApJ*, 443, 209
 Beck, R. 2000, *Space Sci. Rev.*, 99, 243
 Bell, A. R. 1978, *MNRAS*, 182, 147
 Bell, A. R. 2004, *MNRAS*, 353, 550
 Blandford, R. D., & Ostriker, J. P. 1978, *ApJ*, 221, 29
 Clarke, D. A. 1996, *ApJ*, 457, 291
 Clarke, D. A., Norman, M. L., & Burns, J. O. 1989, *ApJ*, 342, 700
 de Avillez, M. A., & Breitschwerdt, D. 2007, *ApJ*, 665, 35
 DeLaney, T., Koralesky, B., & Rudnick, L. 2002, *ApJ*, 580, 914
 Dickel, J. R., Breugel, W. J. M., & Strom, R. G. 1991, *AJ*, 101, 2151
 Dickel, J. R. & Milne, D. K. 1976, *Australian Journal of Physics*, 29, 435
 Drury, L. O'C. & Falle, S. A. E. G. 1986, *MNRAS*, 223, 353
 Fraschetti, F. 2013, arXiv:1304.4956
 Giacalone, J., & Jokipii, J. R. 2007, *ApJ*, 663, 41
 Guo, F. et al. 2012, *ApJ*, 747, 98
 Jun, B.-I., & Norman, M. 1996, *ApJ*, 472, 245
 Inoue, T., Yamazaki, R., & Inutsuka, S. 2009, *ApJ*, 695, 825
 — 2010, *ApJ*, 723, L108
 Inoue, T., Yamazaki, R., Inutsuka, S., & Fukui, Y. 2012, *ApJ*, 744, 71
 Inoue, T., & Inutsuka, S. 2012, *ApJ*, 759, 35
 Inoue, T. 2012, *ApJ*, 760, 43
 Malkov, M. A., Diamond, P. H., & Sagdeev, R. Z. 2010, *PPCF*, 52, 124006
 Mikaelian, K. O. 1996, *Phys. Fluids*, 8, 1269
 Myers, P. C. 1978, *ApJ*, 225, 380
 Niemiec, J., Pohl, M., Stroman, T., & Nishikawa, K. 2008, *ApJ*, 684, 1174
 Nishihara, K. et al. 2010, *Phil. Trans. R. Soc. A*, 368, 1769
 Reynolds, S. P., & Gilmore, D. M. 1993, *AJ*, 106, 272
 Reynoso, E. M., Hughes, J. P., & Moffett, D. A. 2013, arXiv: 1302.4678
 Richtmyer, R. D. 1960, *Commun. Pure Appl. Math.*, 13, 297
 Riquelme, M. A., & Spitkovsky, A. 2009, *ApJ*, 694, 626
 Schure, K. M., Vink, J., Achterberg, A., & Keppens, R. 2009, *AdSpR.*, 44, 433
 Ohira, Y., Reville, B., Kirk, J. G., & Takahara, F. 2009, *ApJ*, 698, 445
 Ohira, Y., & Takahara, F. 2010, *ApJ*, 721, L43
 Ohira, Y. 2012, *ApJ*, 758, 97
 Sano, T., Inutsuka, S., & Miyama, S. M. 1999, *Numer. Astrophys.*, 240, 383
 Sano, T., Nishihara, K., & Matsuoka, C., & Inoue, T. 2012, *ApJ*, 758, 126
 van Leer, B. 1979, *J. Comput. Phys.*, 32, 101